Journal of
Plant Ecology

Research Article

Asian tropical forests assimilating carbon under dry conditions: water stress or light benefits?

Lian-Yan Yang[1,8], Rui Yu[1], Jin Wu[2], Yongjiang Zhang[3], Yoshiko Kosugi[4], Natalia Restrepo-Coupe[5], Afredo Huete[5], Jie Zhang[1], Yu-Hai Liu[1], Xiang Zhang[1], Wen-Jie Liu[1], Jun-Fu Zhao[1], Jiye Zeng[6], Qing-Hai Song[7], Ya-Jun Chen[7], Liang Song[7] and Zheng-Hong Tan[8,*]

[1]Ecology Program, Department of Ecology, School of Ecology and Environmental Science, Hainan University, Haikou 570228, China, [2]School of Biological Sciences, Faculty of Science, The University of Hong Kong, Pokfulam, Hong Kong, China, [3]School of Biology and Ecology, The University of Maine, Orono, ME 04469, USA, [4]Forest Hydrology Lab, Graduate School of Agriculture, Kyoto University, Kyoto, Japan, [5]School of Life Sciences, University of Technology Sydney, New South Wales, Australia, [6]National Institute for Environmental Studies, Tsukuba, Japan, [7]Xishuangbanna Tropical Botanical Garden, Chinese Academy of Sciences, Menglun, Yunan 666303, China, [8]School of Ecology and Environmental Studies, Yunnan University, Kunming 650091, China

*Corresponding author. Email: tan@ynu.edu.cn

Handling Editor: Bruce Osborne

Received: 16 February 2022, **First Decision:** 12 June 2022, **Accepted:** 25 November 2022, **Online Publication:** 15 December 2022

Abstract

Tropical forests are characterized by vast biomass, complex structures and mega-biodiversity. However, the adaptation processes of these forests to seasonal water availability are less understood, especially those located in the monsoonal and mountainous regions of tropical Southeast Asia. This study used four representative tropical forests spanning from 2° N to 22° N in continental Southeast Asia to address dry-condition photosynthesis at the seasonal scale. We first provided novel and reliable estimations of ecosystem photosynthesis (gross primary production; GPP) seasonality at all four sites. As expected, both evergreen and deciduous seasonal forests exhibited higher GPPs during the rainy season than during the dry season. A bimodal pattern corresponding to solar radiation occurred in the GPP of the perhumid forest. The surface conductance (G_s) was consistently lower both in the dry season and during dry spells (DSPs) than during the wet season and non-dry spells. However, this did not prevent GPP from increasing alongside increasing irradiance in the perhumid forest, suggesting that other ecosystem physiological properties, for example, the light-saturated photosynthetic rate, must have increased, thus surpassing the effect of G_s reduction. Thus, perhumid forests could be defined as light-demanding ecosystems with regard to their seasonal dynamics. Seasonal forests are water-stressed ecosystems in the dry season, as shown by the reductions in GPP, G_s and related ecosystem physiological properties. At all four forest sites, we observed a lack of consistent adaptive strategy to fit the water seasonality due to the diversity in leaf phenology, soil nutrient availability, root depth and other potential factors.

Keywords Eddy covariance, leaf area index, adaptive strategy, ecosystem physiology, gross primary production, latent heat flux, water use efficiency

中南半岛热带森林光合碳同化的季节动态

摘要：热带森林因其生物量巨大、结构复杂和生物多样而著称。然而，关于这些森林光合作用的季节动态及其少水期间的生态适应仍知之甚少。本文利用中南半岛上跨20个纬度(2°–22° N)的自然梯度带，探讨了季节性水分条件变化对中南半岛热带森林光合作用季节动态的影响及其机理。研究结果表明，对于气候季节性明显的热带森林，不论其为常绿、落叶还是半落叶，其雨季的森林冠层光合作用(或称总初级生产总值，GPP)明显高于旱季。缺乏气候季节性的常湿热带雨林，GPP呈现“双峰”季节格局；而且，这种季节格局与太阳辐射之间有较好的对应关系。旱季或者是短干旱期内，冠层导度(G_s)有明显下降，显示出水分对气孔开度的抑制作用。然而，这种气孔开度的降低，并未导致近赤道的常湿低地雨林GPP的下降。也就是说，常湿低地雨林GPP在季节尺度上，表现为光限制而非水分限制。气候季节性明显的3个站点，不论G_s还是GPP在旱季明显低于雨季，则表现出明显的水分限制。

关键词：涡度相关法，叶面积指数，适应对策，生态系统生理，总初级生产力，潜热通量，水分利用效率

INTRODUCTION

Plants are bounded to certain spaces and are selected to fit the surrounding abiotic (i.e. climate and soil) and biotic environments (i.e. the neighboring organisms, local herbivores and microbial communities). Equatorial tropical forests do not experience strong seasonal variations in temperature because of the year-round high solar elevation angle. They do, however, experience rainfall variabilities with either predictable seasonality or irregular dry spells (DSPs). How tropical forests adapt to these regular or irregular rainfall variations is still actively debated (Saleska *et al.* 2016).

This debate initially focused on the phenology of forests with climatic seasonality (cf. Eamus and Prior 2001; Leigh 1999 and references therein). Significant changes in leaf phenology were not observed in most trees when researchers watered two 2.25-ha plots and maintained the soil water at field capacity throughout the dry season for two years (Wright and Cornejo 1990). This finding violated the traditional hypothesis that water-deficit conditions are the cue for leaf shedding in the late dry season. Further field observations suggested that light is the primary controller of leaf production (Dang *et al.* 2021; Wright and van Schaik 1994). The concept of light-dominated phenology also received support from satellite image analyses. Huete *et al.* (2006) found that the vegetation index of Amazon rainforests increased by 25% with increased sunlight during the dry season. Myneni *et al.* (2007) stated that not only the leaf phenology but also the leaf area index increased in the dry season under optimal light conditions. The leaf phenology seasonality could also be accounted for by the herbivore pressure escape hypothesis (Aide 1992). This hypothesis suggests that minimal insect activity co-occurs with maximal irradiance in the relatively dry season, thus reducing the pressure selection for dry-season leaf production.

The debate was extended to dry-season carbon assimilation in the early 2000s. Although direct ecosystem flux measurements in tropical forests began in the late 1980s with ECtechniques (Fan *et al.* 1990; Grace *et al.* 1995), multiyear and cross-season observations were not reported until 10 years later (Goulden *et al.* 2004; Saleska *et al.* 2003). The eddy flux measurements revealed a novel (unexpected) seasonal pattern indicating enhanced photosynthesis in the dry season. Satellite images show that this unexpected pattern was not a site-specific phenomenon but instead a regional one (Huete *et al.* 2006; Xiao *et al.* 2005). These findings supported the new hypothesis that tropical forests are light-controlled (Graham *et al.* 2003) rather than water-limited, even during the dry season. If these hypothesis were validated, the predicted increases in drought frequency and intensity (Chadwick *et al.* 2016) would substantially benefit carbon assimilation in tropical forests. In other words, tropical forests would be drought-resilient (Phillips *et al.* 2009).

The light-limitation hypothesis was soon found to be unsuitable for application to all global tropical forests. Even in the tropical Amazon, only a narrow band (defined as 5° N–5° S) of equatorial forests was found to be light controlled (Restrepo-Coupe *et al.* 2013). A global analysis that included the Amazonian, Southeast Asian and African tropical forests demonstrated that an annual rainfall threshold value of 2000 mm can be used

to categorize tropical forests into two groups: light-controlled and water-limited tropical forests (Guan *et al.* 2015). This 2000-mm threshold was supported by the compilation of independent inventory datasets (Wagner *et al.* 2016).

The embodied mechanism of the light-limitation hypothesis is mainly based on two aspects, namely deep water usage and enhanced light-use efficiency in the dry season. The roots of Amazon forest trees can reach up to 8 m deep (Nepstad *et al.* 1994) and 12 m deep (Brum *et al.* 2018). Significant soil water changes have been observed at depths of 4–8 m during the dry season, indicating that plant use water from soils at these depths (Jipp *et al.* 1998). Markewitz *et al.* (2010) and Davidson *et al.* (2011) quantified the water use at different soil depths in a throughfall exclusion experiment and showed that 10% of water was used from the 5.5–11.5-m soil column and 20% was used from the 2.5–5.5-m column. Thus, deep soil water usage is substantial and plays a significant role in plants overcoming dry conditions, at least in Amazonian forests.

The idea of enhanced light-use efficiency has been supported by several different pieces of evidence. Taking into account the well-known relationship between photosynthesis and leaf age (Kikuzawa 1991; Kitajima *et al.* 1997), Wu *et al.* (2016) reproduced seasonal ecosystem photosynthesis data and found a strong correlation with the photosynthesis capacity, as derived from the seasonally varied canopy leaf age composition (r = 0.96). Newly flushed leaves in the early dry season matured and reached a high photosynthetic potential, resulting in a high level of photosynthesis in the late dry season and the early rainy season (Lopes *et al.* 2016). In addition to spaceborne LiDAR (Light Detection and Ranging) data, Tang and Dubayah (2017) attributed enhanced dry-season photosynthesis to changes in the vertical canopy structure. The abscission of old upper-story leaves provides an additional opportunity for newly flushed understory leaves to achieve high photosynthetic performances. Yan *et al.* (2017) provided simulated evidence to illustrate that enhanced photosynthesis in the late dry season is partly due to an increase in the diffusive radiation fraction. In addition, leaf flushing could also be explained in the context of the hydraulic segmentation hypothesis (Bucci *et al.* 2016). Leaves experience the lowest water potential among plant organs. Therefore, if their vulnerability to cavitation is the same as or greater than that of the more central plant organs (e.g. the main stem), peripheral organs such as leaves will cavitate before the central organs do. Thus, hydraulic limits could drive leaf-shedding patterns among tropical trees.

We designed this study to focus on ecosystem photosynthesis (i.e. gross primary production, GPP) in the forests of continental Southeast Asia, aiming to determine whether similar seasonal photosynthesis patterns are observed in the forests of this region with a monsoon climate and mountainous terrain. If this is not the case, it will be important to determine which type of new photosynthesis pattern exists here and what mechanism shapes this seasonal pattern. All of the above unknowns were summarized into the following ecological question: is the carbon assimilation of Asian tropical forests under seasonally dry conditions limited by water stress or benefited by enhanced solar radiation?

METHODS

Framework of this study

Ecosystem photosynthesis alterations can be affected by four major factors: the irradiance, leaf area index, leaf photosynthesis performance and canopy stomatal conductance.

$$\mathrm{GPP} = f\left(Q, LAI, \varnothing_{\mathrm{leaf}}, G_{\mathrm{c}}\right) \quad (1)$$

where GPP is the gross primary production (ecosystem photosynthesis), Q is the irradiance (indicated by photosynthetically active radiation or solar radiation), LAI is the leaf area index, Φ_{leaf} represents the leaf photosynthesis performance and G_{c} is the canopy stomatal conductance. In this study, we discuss all of these factors, but not in an extended fashion. For example, we concentrate on the irradiance rather than the spectrum (the ratio of photosynthetic active radiation) or components (direct or diffusive) when considering the light factor.

Research sites

Mainland Southeast Asia includes Myanmar, Thailand, Peninsular Malaysia, Laos, Cambodia and Vietnam. The major forest types in this region include lowland tropical rainforests, tropical dry evergreen forests, mixed deciduous forests and deciduous dipterocarp forests. The four selected sites and their general descriptions are shown in Fig. 1.

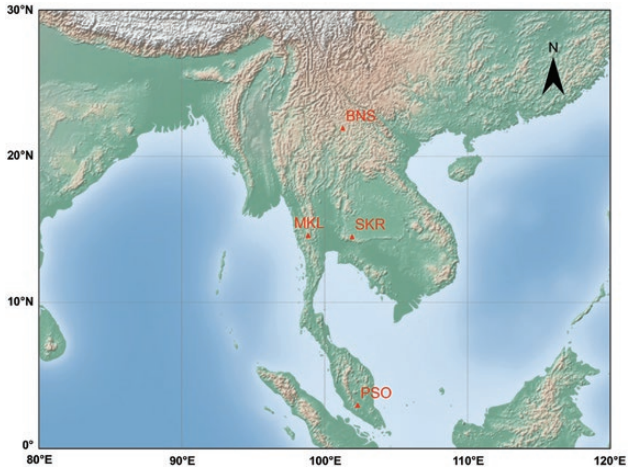

Figure 1: Site map.

Xishuangbanna Ecological Station, China (BNS site)

The BNS site was the northernmost site among the four selected sites. This site is located close to the Tropic of Cancer and is regarded as the northernmost fringe of Southeast Asia's tropical forests. The day length, solar radiation and temperature are relatively low in winter, owing to the relatively high latitude of this area. According to China's vegetation classification system, the 'tropical seasonal rainforest' forest type is found at the BNS site (Cao *et al.* 2006; Hou 1983; Zhang and Cao 1995). This name has two implications: first, the forests are true lowland tropical rainforests (Cao *et al.* 2006); second, the forests exhibit strong seasonality in both the climate and ecological processes, in contrast to equatorial rainforests. The BNS site has had long-term ecological monitoring (permanent plots with soil, forest hydrology and climate measurements) since the early 1990s. The mean annual temperature and annual precipitation are approximately 21.8°C and 1493 mm, respectively. The climate of this site is strongly seasonal and can be divided into three subseasons, namely the cool-dry (November to February), hot-dry (March and April) and rainy (May through October) subseasons (Zhang 1963). Dense fog frequently occurs from morning to midday during the cool-dry season. The soils are of the laterite type and are developed from siliceous rocks; the soils have a deep solum, a thin humus horizon and a pH value of 4.5–5.5 (Cao *et al.* 2006). The canopy is uneven, with a closed canopy height of approximately 30 m. Buttresses, epiphytes, lianas and stranglers are abundant in this forest. The canopy can be divided into three layers, namely the emergent layer (>30 m), major canopy layer (21–30 m) and understory (5–20 m) (Zhang and Cao 1995). The typical canopy tree species are *Pometia tomentosa*, *Terminalia myriocarpa* and *Semecarpus reticulata*. The soil organic matter content is 32.2 g kg^{-1}; the available nitrogen content is 165.2 mg kg^{-1} and the available phosphorus content is 2.51 mg kg^{-1} (Fang and Sha 2006).

Sakaerat Environmental Research Station, Thailand (SKR site)

The SKR site is located at the edge of the Khorat Plateau in northeastern Thailand. The plateau has relatively simple geology and topography and covers nearly one-third of Thailand. The typical vegetation type in this area is tropical dry evergreen forests (Rundel and Boonpragob 1995). Floristically, the dry evergreen forests could be viewed as an extension of the Malaysian rainforests. The study site was established in 1967 by the Royal Forestry Department and is administered by the Thailand Institute of Scientific and Technological Research (https://www.tistr.or.th/sakaerat/); this site has been listed as a UNESCO Biosphere Reserve since 1977. Although the canopy is evergreen, the mean annual precipitation is as low as 1200 mm (1132-mm average from 1967 to 1970, as cited from Pinker *et al.* (1980); 1240-mm average from 1969 to 1982, as cited from Rundel *et al.* (2017); 997-mm average from 1982 to 2001, as cited from Suriyapong (2003); 1222-mm average as cited from Yoda and Nishioka (1982)). Over 80% (1114 mm in Yoda and Nishioka (1982); 1003 mm in Rundel *et al.* (2017); 793 mm in Suriyapong (2003)) of precipitation occurs during the rainy season (from May through October), while sunny rainfall events also occur in March and April (Supplementary Fig. S1). The mean annual temperature is approximately 26.4°C (averaged from 1982 to 2001 (Suriyapong 2003)). The highest and lowest monthly mean temperatures were reported to be 29.6°C (April) and 21.7°C (December), respectively. The soils are shallow (with a mean soil depth of 79 cm (Murata *et al.* 2009)), acidic (pH = 4.5) and nutrient-poor (with a total nitrogen content of 1.86 g N kg^{-1} (top 5 cm) (Ueda *et al.* 2017) and available phosphorus content of 5.3 mg kg^{-1} (Rundel and Boonpragob 1995)) stony Ultisols. The dense canopy is continuous and closed at a height of 20–35 m (upper canopy), and the canopy usually intercepts over 80% of the light (Yoda *et al.* 1983). The second stratum, ranging from 5 m to 17 m, is relatively open. The understory is dense and rich in lianas. The canopy is dominated by *Hopea ferrea*.

Maeklong Watershed Research Station, Thailand (MKL site)

The typical vegetation type at the MKL site is tropical dry deciduous forests (Marod *et al.* 1999). The annual rainfall (1635 mm averaged from 1995 to 2001, as cited from Suksawang *et al.* 2001; 1761 mm averaged from Terakunpisut 2003) is higher than that at the SKR site and is mainly distributed during the rainy season (May through October). Similar to the BNS and SKR sites, the dry season at the MKL site can be divided into two subseasons, namely the cool-dry and hot-dry subseasons. Approximately 61% of water evaporates at this site and the rest leaves the ecosystem as runoff or leakage (Suksawang *et al.* 2001). The mean temperature is 27.5°C with a large annual range (maximum, 39.1°C in April and minimum, 14.6°C in December). The Alfisols are relatively deep (at least 160 cm, Takahashi *et al.* 2011), and the MKL site has higher pH values (5.7–7.1) and richer in nutrients (total nitrogen: 2.13 g N kg^{-1} (top 5 cm, Takahashi *et al.* 2011); available phosphorus: 16.8 mg kg^{-1}, Rundel and Boonpragob 1995) than the SKR site. Here, the canopy at this site has three strata, namely the upper canopy, medium layer and lower layer are found at heights of 25–30 m, 10–25 m and <10 m, respectively (Bunyavejchewin 1983). The dominant canopy species include *Shorea siamensis*, *Vitex peduncularis* and *Xylia xylocarpa*.

Pasoh Forest Reserve, Peninsular Malaysia (PSO site)

The PSO site is closer to the equator than the other sites. The annual rainfall at this site is 1804 mm (averaged from 1983 to 1997) and is relatively evenly distributed among the months (Yada and Kira 1982). The lowest monthly rainfall occurs in January (near 100 mm), whereas the highest occurs in November (above 200 mm, Kosugi *et al.* 2008). No clear or predictable dry season can be discerned at this site based on either rainfall or soil water records (Kosugi *et al.* 2012). Short DSPs do occur, during which the forest floor is dried up (Yada and Kira 1982). The mean annual temperature is 25.3°C, and the highest mean temperature has been recorded at 26.1°C in April, with the lowest temperature of 24.3°C recorded in December (collected at an approximately 53-m height, averaged from 2003 to 2009). The Ultisols are deep but poor in nutrients (total nitrogen, 1.72 g N kg^{-1}; available phosphorus, 3.5 mg kg^{-1} for the A horizon, Yamashita *et al.* 2003). The closed canopy reaches a height of approximately 25–35 m, with some emergent trees reaching as high as 50–60 m (Yada and Kira 1982). The small tree and shrub layer is not well defined, as shown by the continuous light interception in this range (Yoda 1983). The canopy is composed mainly of Dipterocarpaceae trees, especially *Shorea* and *Dipterocarpus*.

Determination of GPP

We used the eddy covariance (EC) technique to compute the GPP. Currently, EC might be the only direct way to measure mass and energy exchanges between entire tall forest ecosystems and the atmosphere without inducing inevitable artificial impacts. The eddy flux provides the net ecosystem exchange (*NEE*) instead of the GPP. According to atmospheric turbulence theory (Swinbank 1951), the *NEE* can be calculated using high-frequency (usually 10-Hz) vertical wind velocity (w) and scalar (c, here specified to CO_2) density data recorded with a storage flux (F_s) correction (Grace *et al.* 1995):

$$NEE = F_c + F_s = \rho\overline{\langle w'c'\rangle} + \frac{d\int_{z=0}^{z=h} C_a(z)\mathrm{d}z}{dt} \qquad (2)$$

where F_c is the carbon flux transferred by the eddies, F_s is the flux related to variations in stored CO_2 in the air column, ρ is the air density and the overbar indicates the time average and the primes represent fluctuation (which is the difference between the record and the average), h is the sensor height, $C_a(z)$ is the CO_2 concentration as a function of height (z) and dt is the time interval used for averaging, usually 30 min.

In principle, GPP can be inferred (usually 'partitioned') from *NEE* as follows:

$$\mathrm{GPP} = -(NEE - R_e)_{\mathrm{day}} \qquad (3)$$

where R_e is the ecosystem respiration and the 'day' outside the parentheses denotes daytime. Two major methods can be used for GPP partitioning, namely the nighttime method (Reichstein *et al.* 2005) and the daytime method (Lasslop *et al.* 2010). The nighttime method has been criticized for overestimating the GPP since it does not account for light inhibition of respiration caused by the Kok effect (Keenan *et al.* 2019; Wehr *et al.* 2016). The general ideas for both the nighttime and daytime methods are shown below. Details can be obtained in the references of Reichstein *et al.* (2005) and Lasslop *et al.* (2010).

Nighttime method

Light is not available during the nighttime. Under such circumstances, the postprocessed *NEE* can be

viewed directly as the ecosystem respiration. Then, the site-specific relationships between the nighttime *NEE* and environmental factors, especially soil temperature, can be established. These relationships can then be used to extrapolate the daytime respiration (Reichstein *et al.* 2005).

Daytime method

The daytime *NEE* is the net balance between photosynthesis and the daytime respiration. Relating the daytime *NEE* to the light intensity and other environmental factors can help us estimate the *NEE* when the amount of light theoretically approaches zero (most frequently via a hyperbola equation) (Lasslop *et al.* 2010).

Flux data were collected from the AsiaFLUX database (https://db.cger.nies.go.jp/asiafluxdb/). The instrumentation, sampling frequency and measurement heights are explained in detail in the dataset. The collected datasets were submitted to an online flux-processing program maintained by MPI to undergo both u*-screening and flux partitioning (https://www.bgc-jena.mpg.de/bgi/index.php/Services/REddyProcWeb). The online program provided GPP estimates for the BNS, MKL and PSO sites but not for the SKR site. The GPP estimates of the BNS and PSO sites from the online program were 11.4 and 17.1 t C ha^{-1} $year^{-1}$, respectively; these values were unreasonable. Thus, the GPP of only the MKL site was adopted after online processing in this study. Site-specific algorithms were adopted for the flux partitioning of the other three sites.

SKR site

The daytime method was adopted for the SKR site. We related the daytime *NEE* to the light intensity, temperature and water vapor deficit as described by Lasslop *et al.* (2010) (cf. Chen *et al.* [2019] for details of the equations and fitted parameters). A close relationship was found between the dark respiration (the daytime ecosystem respiration extrapolated to zero light, R_d) and water vapor deficit (cf. Supplementary Figs S2 and S3). Carbon flux partitioning was accomplished with the specific relationship obtained for the SKR.

PSO site

As stated by Kosugi *et al.* (2008), the nighttime *NEE* was largely underestimated even after u*-screening with a relatively high threshold at the PSO site (cf. page 445 of Kosugi *et al.* (2008) for more details). Kosugi *et al.* (2012) provided a nighttime-based GPP estimation method by linking the 'optimum' nighttime *NEE* to the soil water content. Here, we provide a new daytime-based GPP estimation method. Initially, a mean dark respiration (R_d) value of 5.4 μmol m^{-2} s^{-1} was derived through the link between the daytime *NEE* and light intensity. This value was consistent with the nighttime *NEE* values, suggesting that '*…the nocturnal CO_2 flux can be measured with the EC method over the canopy in correspondence only with the soil respiration component estimated with the chamber method…*' (Kosugi *et al.* 2008). After careful examination, we found that weak light records contaminated the R_d estimations (cf. Supplementary Figs S4 and S5). After excluding the data obtained under weak light conditions (solar radiation under 20 w m^{-2}), the daytime method-derived R_e values were very close to the optimum value reported by Kosugi *et al.* (2012) in their annual sums. Thus, we used the dataset in which weak light conditions were omitted to perform curve fitting at a monthly interval for seven years to obtain R_d estimates. The year-based mean values of the seven-year data were averaged into one year to represent the seasonality of respiration.

BNS site

The daytime method failed in the hot-dry subseason (March and April) at the BNS site (cf. Supplementary Fig. S6). Thus, the nighttime method was used for this site. The nighttime flux was related to the air temperature after the exclusion of spikes and u*-screening with the following equation:

$$R_e = R_0 Q_{10}^{(T_a - T_0)/10} \quad (4)$$

where R_0 and T_0 are fitted parameters, T_a is the air temperature and Q_{10} is set with regards to soil respiration (Sha *et al.* 2005).

Light intensity and other climatic factors

There are extensive recordings of climatic factors accompanied by flux measurements. We used solar radiation (R_g) to represent the irradiance. The instrument model consistently used for R_g is the CNR net radiometer (Kipp&Zonen, Delft, Netherlands). We used the downward shortwave radiation measured by CNR as solar radiation (R_g). To clarify the effect of cloud cover on R_g, we also calculated the clear-day R_g for all sites. The MATLAB code for clear-day R_g was calculated with self-coding based on Campbell and Norman's (1998) equations (the code is provided in the Supplementary Code S1 and Fig. S7). Instrumentation details regarding

the other climatic factors are available from the AsiaFLUX database.

LAI and leaf photosynthetic performance

We used the Beer–Lambert Law to estimate the empirical LAI as per the method described by Monsi and Saeki (2005):

$$\mathrm{LAI} = -\frac{\ln(Q_i/Q_0)}{k} \tag{5}$$

where Q_i and Q_0 refer to the average PAR below (near the forest floor) and above the canopy, respectively and k is the light extinction coefficient. We set k to 0.55 according to Jarvis and Leverenz (1983), who suggested a value range of 0.5–0.8 for broadleaved forests. We first calculated the daily mean Q_i and Q_0 values. Then, we calculated the LAI based on the daily binned value to reduce variability. Spikes were removed with reference to the method of Gamo and Penuthai (2005), the litterfall data, and the satellite image values (cf. Supplementary Figs S8 and S9). We also collected the satellite LAI at a 1-km spatial resolution every 10 days from 1999 to 2008 from the Copernicus Global Land Service (https://land.copernicus.eu/global/themes/vegetation). Because the Q_i values were not available for the PSO site, we used the satellite LAI values instead.

A new term, called unit leaf photosynthesis (Λ_{unit}), was proposed to serve as an approximation for the leaf photosynthetic performance (Φ_{leaf}). Λ_{unit} can be defined as follows:

$$\Lambda_{unit} = \frac{\mathrm{GPP}}{LAI} \tag{6}$$

where Λ_{unit} is the GPP normalized to the *LAI*. When the Λ_{unit} term is used to investigate the reason for the GPP seasonality, the change in the number of leaves, which is usually measured from satellite images, can be ruled out. Conceptually, Λ_{unit} includes information on all leaf photosynthetic properties: the quantum yield, carboxylation rate and leaf stomatal conductance.

Surface conductance

The canopy surface conductance (G_s) was calculated by inverting the Penman–Monteith equation as follows (Supplementary Fig. S10):

$$G_s = \left[\frac{\rho C_p}{\gamma}\frac{D}{\lambda E} + \left(\frac{\Delta}{\gamma}\frac{H}{\lambda E} - 1\right)\left(\frac{1}{G_{aV}}\right)\right]^{-1} \tag{7}$$

where λE and H are the latent and sensible heat fluxes, respectively; D is the water vapor deficit; C_p is the specific heat capacity of air; γ is the psychometric constant and G_{aV} is the aerodynamic conductance of water vapor. More information is available from Tan *et al.* (2019) and in the Supplementary Code S2. For dense closed canopies, the dry-canopy G_s can be roughly used as an indicator of the canopy conductance (G_c), which represents the bulk canopy leaf stomatal conductance.

Evapotranspiration and water use efficiency

Photosynthesis is coupled to transpiration through the stomata of leaves. Guan *et al.* (2015) demonstrated that the photosynthetic seasonality of tropical forests is controlled mainly by the water budget at the global scale. Thus, we included the evapotranspiration (ET) and water use efficiency (WUE) to obtain a better understanding of the GPP seasonality. The latent heat flux (λE) provided by the EC system was used without applying an energy balance closure correction. The data gaps were filled with the mean diurnal variation method. The *ET* values were converted from λE as follows: $ET = \lambda E/\lambda$, where λ = 2260 kJ kg^{-1}. The WUE here was defined as the ratio between the GPP and ET.

Ecosystem physiology

We focused on three ecosystem physiological properties: the apparent quantum yield (α), light-saturated photosynthesis rate (P_{max}) and sensitivity of G_s to D (m'). These parameters were obtained by curve fitting as follows (Supplementary Code S3, S4 and Figs S3, S5, S6, S11–S15):

$$-NEE_{day} = \frac{\alpha P_{max} Q}{\alpha Q + P_{max}} - R_d \tag{8}$$

$$G_s = G_{smax}\left(\frac{Q}{Q+Q_0}\right)(1 - m'\ln(D)) \tag{9}$$

where NEE_{day} is the daytime *NEE* value defined as R_g above 2 w m^{-2}; the negative sign before NEE_{day} is the result of the discipline convention, which defines a flux into the ecosystem as negative in Cartesian coordinates; and G_{smax}, Q_0 and m' are three fitted parameters. The m' value used here differs from that applied in Oren *et al.* (1999) but can roughly serve as a sensitivity index when exploring the G_s–D relationship (Supplementary Fig. S16).

In the case that D = 1 kPa, G_s is independent of D:

$$G_s = G_{smax}\left(\frac{Q}{Q+Q_0}\right) \tag{10}$$

In the case that $D > 1$ kPa, $\ln(D) > 0$ and the decrease rate of G_s with increasing D is dependent on m'.

Actually,

$$\frac{\partial G_s}{\partial D} = -G_{smax}\left(\frac{Q}{Q+Q_0}\right)\frac{m'}{D} \quad (11)$$

thus, we regarded m' as an approximate sensitivity index in this study.

We defined the seasons characteristic of each site using the seasonal climate data and DSPs for the perhumid PSO site for the ecosystem physiology analysis. For the seasonal sites, we first defined the rainy season as the period from May through October. Then, we defined March and April as the hot-dry subseason. During this period, the air temperature (T_a) reached its highest point along with solar radiation (R_g) and the water vapor pressure deficit (D). The other part of the dry season was categorized as the cool-dry subseason. For the perhumid PSO site, the DSPs were defined according to both the precipitation and soil water content. Details are provided in the Supplementary Fig. S17. For comparison, the non-DSP period was defined as the period 15 days before and 15 days after the DSP for the pairwise comparison.

Simulations

To separate the contributions of the ecosystem properties or climate conditions to the GPP, we simulated the GPP in two dependent ways. This simulation was performed only at the SKR site, where the dry season was clear with enhanced light but the evergreen canopy was maintained. We selected the hot-dry period (March and April) and mid-late rainy season (August and September) to represent the light-enhanced (dry) and water-stress-free (rainy) stages, respectively (cf. Supplementary Fig. S18).

First, the GPP was expressed as a function of Q:

$$\mathrm{GPP} = \frac{\alpha P_{max} Q}{\alpha Q + P_{max}} \quad (12)$$

Six scenarios were set: scenario 1, the 'rainy'-stage α driven by Q in the 'dry' period (α+); scenario 2, the 'rainy'-stage P_{max} driven by Q in the 'dry' period (P_{max}+); scenario 3, the 'rainy'-stage α and P_{max} driven by Q in the 'dry' period (α+ &P_{max}+); scenario 4, the 'dry'-stage α driven by Q in the 'rainy' period (α-); scenario 5, the 'dry'-stage P_{max} driven by Q in the 'rainy' period (P_{max}-); and scenario 6, the 'dry'-stage α and P_{max} driven by Q in the 'rainy' period (α- &P_{max}-) (the relevant code is included in supplementary material).

Second, the GPP was expressed as a function of G_s (Medlyn *et al.* 2011):

$$\mathrm{GPP} = \frac{C_a}{1.6}\frac{\sqrt{D}}{\sqrt{D}+g_1}G_s \quad (13)$$

where the expression of G_s is shown in Equation (9), C_a is the carbon dioxide concentration of air (ppm), g_1 is set as 2.8 according to Wu *et al.* (2020), G_s is in m s^{-1}, D is in kPa and g_1 is in sqrt(kPa). A coefficient [1.7867 (kg m^{-3}) × 1000 (g kg^{-1})/44(g mol^{-1})] was multiplied by GPP to change the unit to μmol m^{-2} s^{-1}. Three scenarios were set: scenario 1, the 'rainy'-stage G_{smax} driven by Q, D, and C_a in the 'dry' period (G_{smax}+); scenario 2, the 'rainy'-stage m' driven by Q, D, and C_a in the 'dry' period (m'+) and scenario 3: the 'rainy'-stage G_{smax} and m' driven by Q, D, and C_a in the 'dry' period (G_{smax}+ &m'+) (the relevant code is included in Supplementary Code S4 and S5).

RESULTS

Climate and LAI

The seasonality of the climate variables increased with latitude among the four sites (Fig. 2). The precipitation (PPT) seasonality differed largely among the sites; precipitation was relatively evenly distributed among months at the PSO site. The PPT seasonality was strongest at the MKL site, where nearly no PPT occurred during the three-month dry period (December to February). The monthly mean air temperature (T_a) was 15°C at the end of the year for the northern BNS site, while this value was higher than 22°C at the other sites. Solar radiation was highest in the late dry season (March and April) at all four sites. This seems to be a regional property in continental Southeast Asia and was part of the reason for us defining the hot-dry subseason. The monthly R_g of the sites was higher than 300 MJ $month^{-1}$ since a continuous high solar energy input is important for maintaining the tropical climate. A similar pattern between R_g and D was observed at all four sites with either seasonal or perhumid conditions. This could easily be explained because an increase in R_g indicates an increased temperature and reduced humidity and precipitation.

We plotted the observed values and calculated the daily solar radiation to illustrate the contribution

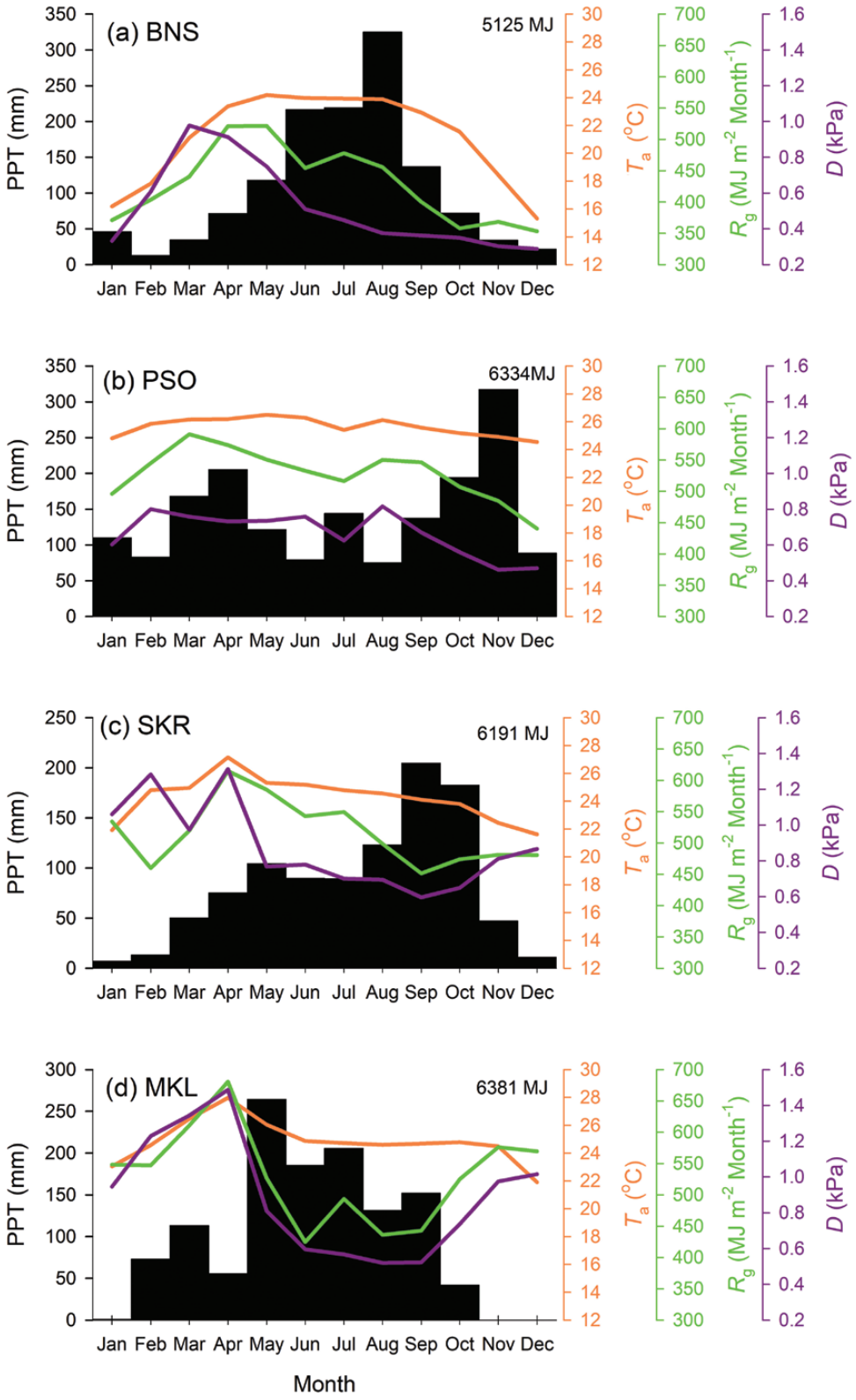

Figure 2: Climate diagrams at the BNS site (**a**), PSO site (**b**), SKR site (**c**) and MKL site, respectively. Monthly averaged value for two or three years (detailed time periods are available in the text). The bars are precipitation (PPT); the lines are the air temperature above the canopy (T_a), solar radiation (R_g) and the water vapor deficit (D), respectively. Please note that the PPT data from the SKR site represent averaged values from 1982 to 2001.

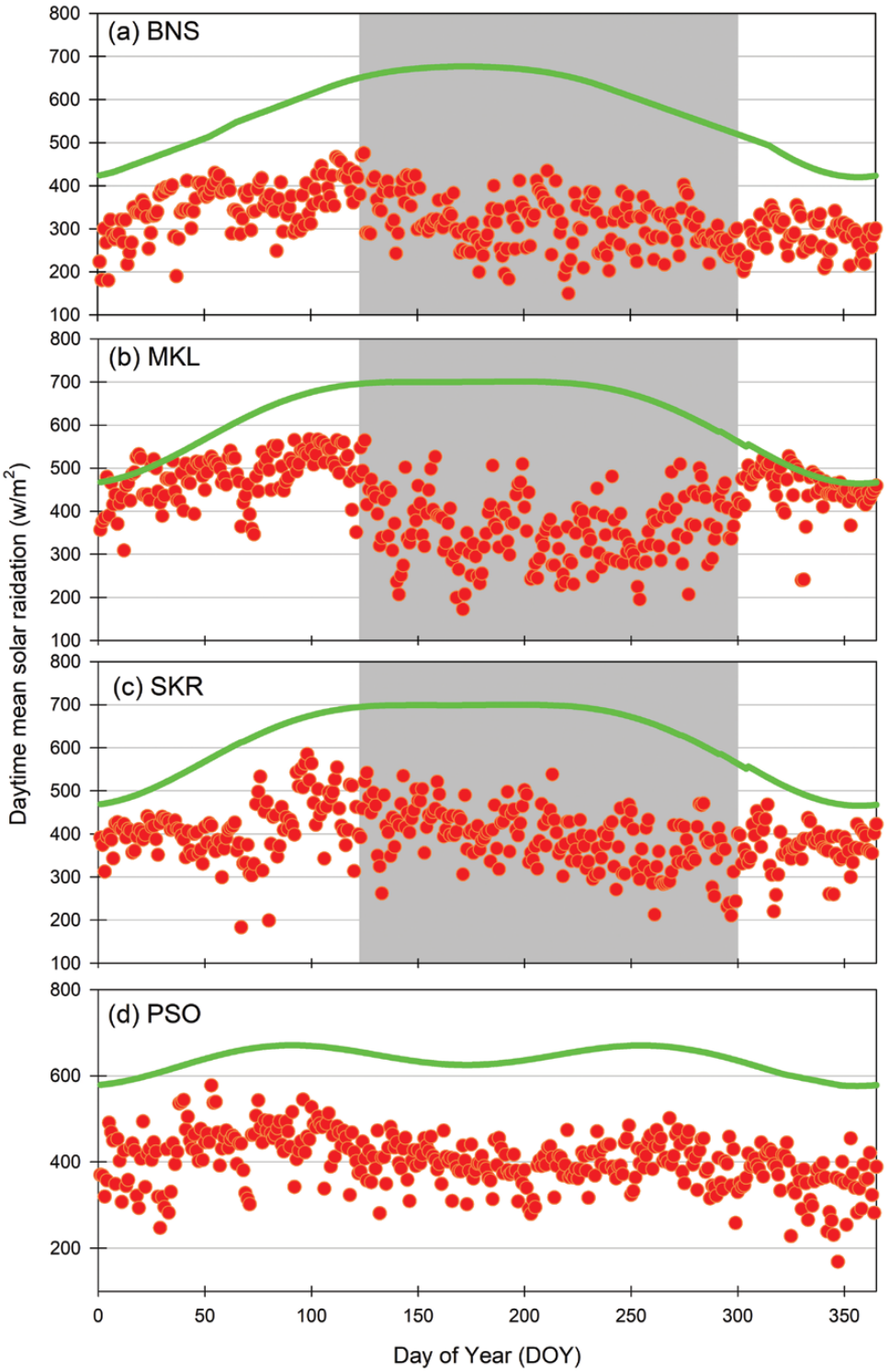

Figure 3: Averaged annual variation in solar radiation for both observed (circles) and calculated (line) values with daily intervals at the BNS site (**a**), MKL site (**b**), SKR site (**c**) and PSO site, respectively. The shaded area indicates the rainy season.

of cloud cover (Fig. 3). Interestingly, in the dry-hot period, R_g was not captured by the sun–Earth geometry-based calculated value (Fig. 3); that is, this pattern could be related to other local climate properties, such as the clarity of the sky, temperature and humidity-related radiation balance. The rainy-season reduction in R_g was higher than the calculated values at the MKL site due to the concentrated rainfall during that period. In contrast, rainfall properties such as the local rainfall time, rainfall intensity and

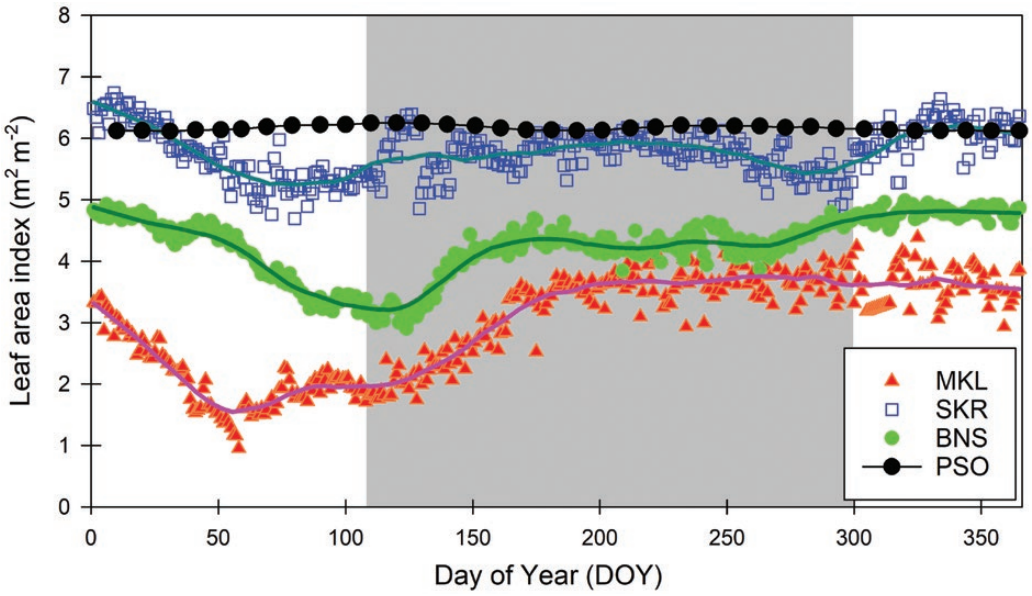

Figure 4: LAI calculated based on light transmittance at the BNS, MKL and SKR sites. Data for the PSO site were collected from satellite images. The shaded area indicates the rainy season.

duration could also play important roles. A bimodal curve occurred for R_g at the PSO site despite the recorded high precipitation in the corresponding bimodal periods.

Almost no seasonal variation in LAI was observed in the perhumid forest of PSO, as shown in the satellite image (Fig. 4). The 20-year results (1999–2008) show that the LAI of the PSO site nearly stabilized at approximately 6.1 m^2 m^{-2}. The dry evergreen forest at the SKR site, however, did not seem to be strictly evergreen. The light transmittance exhibited two low-LAI periods: the hot-dry period and the end of the rainy season, with the first period regularly showing low LAI values every year and the second period showing low values only in 2002 and 2003. We addressed the details of these variations from the findings of Gamo and Penuthai (2005; Fig. 5 therein). The first regular low-value period in the dry-hot season might be related to water stress. We do not have strong evidence to explain the cause of the second irregular period. The LAI was usually higher than 5 m^2 m^{-2} despite the low-light-transmittance periods at the SKR site. This indicated that these variations were relatively small compared to those at the other deciduous or semideciduous forest sites. The trees at both the MKL and BSN sites started shedding leaves at the end of and/or the beginning of each year. The shedding rates and durations differed between the two formations, with higher leaf-shedding observed at the MKL site than at the BNS site. Moreover, at the MKL site, the leaves shed very quickly and reached their lowest value before the beginning of the dry-hot season, followed by slow leaf flushing, growth and maturation. The BNS trees shed leaves slowly, but the subsequent leaf-flushing and growth periods were relatively rapid.

Ecosystem flux

Fig. 5 shows the annual variations in the latent heat flux (λE), gross primary production (GPP) and water use efficiency (WUE) at the four study sites. Different patterns occurred between the λE and GPP results, although these processes should be coupled. This finding suggests that the λE and GPP might be controlled by different environmental factors, at least at the annual scale. The λE results of the BNS site showed a similar pattern as the air temperature (T_a). The λE reduction rate was higher than the GPP rate during the cool-dry season. The peak λE occurred in the middle of the rainy season but not in the hot-dry season. Similar to R_g and GPP, λE exhibited a bimodal pattern at the PSO site, where a high λE were maintained year-round and were even higher than the peak value observed at the BNS site in the middle of the rainy season. The λE values at the SKR site were relatively high in the hot-dry season, especially under the relatively low R_g, T_a and D conditions (Figs 2 and 5). Overall, λE was higher in the rainy season than in the dry season, especially in the cool-dry subseason. Although the GPP was relatively low during the

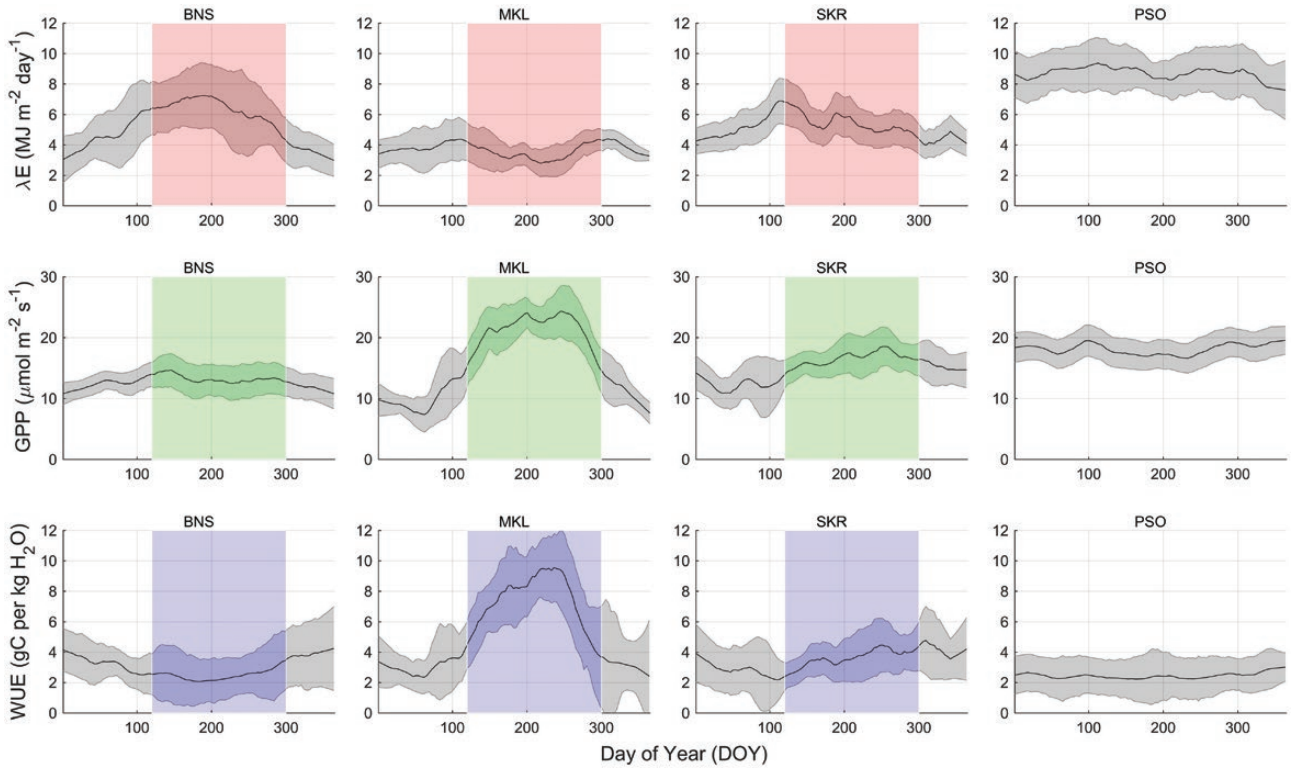

Figure 5: The annual patterns of latent heat flux (λE), gross primary production (GPP) and water use efficiency (WUE). Data were smoothed based on daily values. The grey-shaded area represents the standard deviation. The color-shaded area indicates the rainy season.

leaf-shedding period at the MKL site during the dry season, λE was not (Fig. 5). In addition, the λE results of the MKL site reached the lowest value in the rainy season. The reduction in R_g was higher at the MKL site than at the SKR site (Fig. 3), and this low energy input might have directly affected the subsequent energy driving evapotranspiration. λE was lower at the MKL site than at the other four sites.

The peak GPP value occurred in the early rainy season (day-of-year [DOY] 140–150) at the BNS site (Fig. 5) after the leaf-flushing, expansion and maturity stages. The GPP decreased with decreasing LAI from DOY 60–90, but this trend occurred for only approximately one month. Thereafter, the GPP increased despite the continuous LAI decrease, suggesting that the photosynthesis of the suppressed layers compensated for the leaf loss of the top layer (only tall canopy trees shed leaves during this period). The LAI reached its lowest value at the end of the hot-dry season (DOY 120). Meanwhile, the rapid leaf-flushing, growth and maturity processes maintained high GPP values and led to the maximum GPP value. The decline in GPP after this peak might have been related to the sharp decrease in the light intensity resulting from frequent rain events and cloud cover (Fig. 3). Moreover, the relatively low GPP in the cool-dry season could be explained by both the relatively low radiation and temperature conditions (Fig. 2). The annual GPP pattern was bimodal but varied slightly at the PSO site (Fig. 5), and a similar bimodal trend was observed for solar radiation (Fig. 3). The annual GPP variation was highly correlated with the vegetation index (EVI) at the SKR site (cf. Supplementary Fig. S19). The GPP seasonality was relatively high at the MKL site (Fig. 5), and this site also exhibited relatively high seasonality in both the rainfall amount and LAI (Figs 2 and 4). The GPP and LAI trends were very similar at the MKL site before DOY 300 (cf. Supplementary Fig. S20).

The WUE was higher in the dry season than in the rainy season at the BNS site (Fig. 5). This factor did not present a bimodal annual pattern at the PSO site (Fig. 5), while both GPP and λE exhibited similar bimodal patterns at the site. The WUE decreased at the beginning of the year at the SKR site and reached its lowest value in the hot-dry season (DOY 120, Fig. 5). Then, it slowly and continuously increased until the end of the year. The WUE seasonality was high at the MKL site (Fig. 5). The relatively high WUE values in the

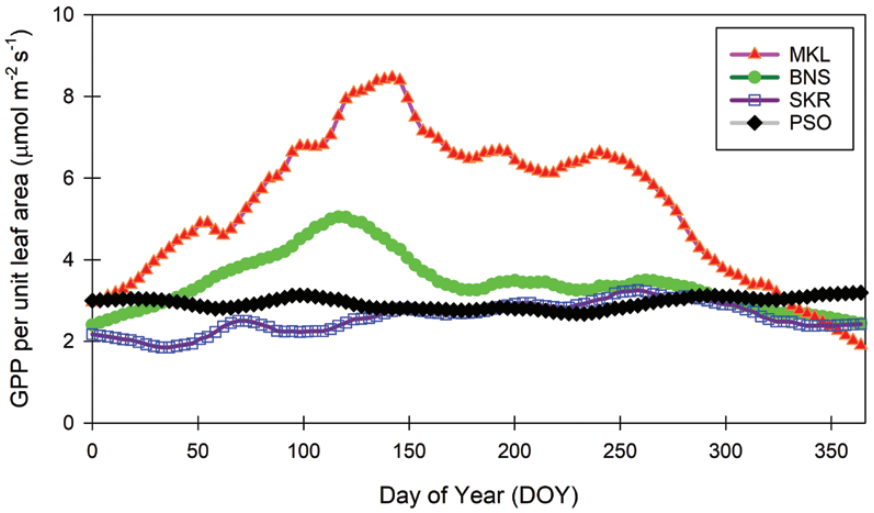

Figure 6: GPP per unit leaf area index (Λ_{unit}) at the BNS (circles), MKL (open squares), SKR (triangles) and PSO (diamonds) sites. The shaded area indicates the rainy season.

rainy season could have been due to the reduced λE enhancing the GPP.

The unit leaf photosynthesis (Λ_{unit}) fluctuated at approximately 3 μmol m^{-2} s^{-1} per unit LAI for the evergreen forests (Fig. 6). Leaf phenology (shedding, flush, growth, maturation and senescence) plays an important role in determining the Λ_{unit}, but different trends were observed between the BNS and MKL sites. A strong relationship between the leaf photosynthetic performance and leaf age (the new leaf benefit; see the discussion section for details) occurred for a short period (almost two months) at the BNS site, but this relationship continued throughout the entire rainy season (even until the dry season) at the MKL site.

Ecosystem physiology

We compared the surface conductance (G_s) values among different seasons in three seasonal forests (Fig. 7a–c). The G_s values were consistently lowest in the hot-dry season (red) and highest in the rainy season (black). Although the lowest λE was observed in the cool-dry season, the G_s of the cool-dry season was as high as that of the rainy season at the BNS site. The λE values were lowest in the rainy season at the MKL site, but the highest G_s was found in the same period at this site.

The mean diurnal G_s patterns at the PSO site during DSP and non-DSP periods are shown in Fig. 7. DSPs significantly reduced the average G_s from 13.03 mm s^{-1} to 9.36 mm s^{-1}. The peak G_s value shifted from the early morning to the early afternoon during DSPs. The effect of DSPs on the reduction in G_s was stronger in the morning than in the afternoon.

The light responses of NEE_{day} are shown in Supplementary Figs. S3, S5, S6 and S11. The parameters are summarized in Table 1 and Fig. 8. P_{max} was significantly higher during the rainy season (34.87 μmol m^{-2} s^{-1}) than during the cool-dry season at the SKR site (24.13 μmol m^{-2} s^{-1}). R_d was significantly higher in the rainy season (8.56 μmol m^{-2} s^{-1}) than in the cool-dry season (4.89 μmol m^{-2} s^{-1}) and hot-dry season (4.74 μmol m^{-2} s^{-1}). No significant differences were observed in the light response parameters among seasons at the BNS site (Supplementary Tables S1–S5). Both α and R_d were significantly lower during DSPs than non-DSPs at the PSO site (Fig. 8). No significant difference was found in P_{max} between DSPs and non-DSPs.

The environmental responses of G_s are shown in the Supplementary Figs S12–S15. The parameters are summarized in Table 2 and Fig. 8. Both Q_0 and m' were significantly higher in the rainy season than in the cool-dry season at the SKR site. No significant difference was observed in any of the G_s response parameters among seasons at the BNS site. The m' values were significantly higher in the hot-dry season than in the cool-dry season at the MKL site. The G_{smax} values were significantly higher during DSPs than during non-DSPs at the PSO site (Fig. 8). No significant difference was found in m' between DSPs and non-DSPs.

Simulations

The light-based GPP simulation results are shown in Fig. 9a and b. Given that α is the same as the 'rainy' stage, the enhanced light in the 'dry' stage contributed

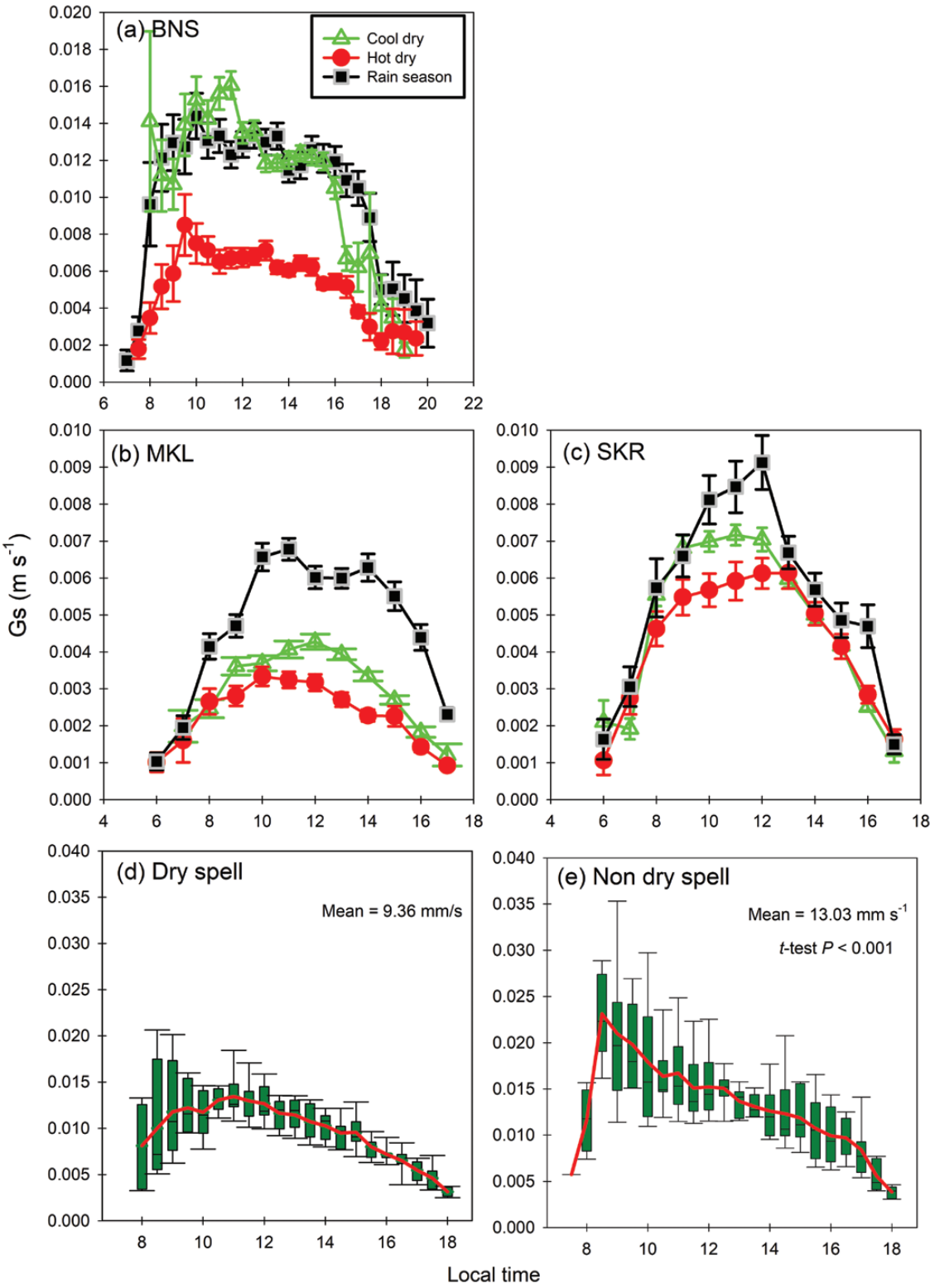

Figure 7: Mean diurnal variations in surface conductance (G_s) under different water conditions: the cool-dry subseason (triangles), hot-dry subseason (circles), rainy season (squares) at the BNS site (**a**), MKL site (**b**) and SKR site (**c**), respectively., dry spells at the PSO site (**d**) and non-dry spells at the PSO site (**e**). Definitions of these seasons and dry spells are provided in the text. The error bars represent the standard errors.

Table 1: Parameters obtained by performing curve fitting on the photosynthetic light response.

Season	Year	α (μmol m^{-2} s^{-1} per w m^{-2})	P_{max} (μmol m^{-2} s^{-1})	*Rd* (μmol m^{-2} s^{-1})	r^2	*n*
MKL						
Cool dry	2003	N.A.	N.A.	N.A.	N.A.	N.A.
	2004	N.A.	N.A.	N.A.	N.A.	N.A.
Hot dry	2003	N.A.	N.A.	N.A.	N.A.	N.A.
	2004	N.A.	N.A.	N.A.	N.A.	N.A.
Rain season	2003	0.163	49.026	11.778	0.402	1779
	2004	0.148	49.694	12.126	0.362	1693
SKR						
Cool dry	2001	0.119	22.596	4.899	0.500	576
	2002	0.138	24.437	5.853	0.481	1514
	2003	0.100	25.366	3.945	0.562	1268
Hot dry	2001	0.125	23.244	4.988	0.726	36
	2002	0.156	9.641	3.902	0.185	401
	2003	0.100	28.315	5.333	0.622	594
Rain season	2001	0.160	30.612	7.728	0.622	1130
	2002	0.162	36.237	8.860	0.651	1775
	2003	0.167	37.762	9.109	0.579	1873
BNS						
Cool dry	2003	0.041	21.817	1.577	0.204	2696
	2004	0.028	32.481	0.005	0.209	2603
	2005	0.040	19.173	1.539	0.131	2689
Hot dry	2003	N.A.	N.A.	N.A.	N.A.	N.A.
	2004	N.A.	N.A.	N.A.	N.A.	N.A.
	2005	0.025	18.697	2.136	0.131	902
Rain season	2003	0.030	26.241	3.109	0.098	3748
	2004	0.035	22.058	3.597	0.067	3932
	2005	N.A.	N.A.	N.A.	N.A.	N.A.

The equation is shown in the text. α: quantum yield; P_{max}: light-saturated photosynthesis rate; R_d: dark respiration; r^2: determinant of coefficient and *n*: number of datasets involved in curve fitting. N.A. indicates that data are not available.

to only a 6% increase in the GPP (scenario 1), while the 'rainy' stage P_{max} driven by the 'dry'-stage light led to a 43% GPP increase (scenario 2). The 'rainy'-stage α and P_{max} driven by 'dry'-stage light had a limited (6%) contribution toward the GPP increase compared to that driven by 'rainy'-stage light (scenario 3). Two points can be easily obtained: first, P_{max} plays a leading role compared to that of α in contributing to an increase in GPP. Second, given the constant ecosystem properties (here α and P_{max}), enhanced light in the 'dry' stage contributed slightly to a GPP increase.

The G_s-based GPP simulation results are shown in Fig. 9c and d. Given that G_{smax} is the same as that in the 'rainy' stage, the enhanced light in the 'dry'

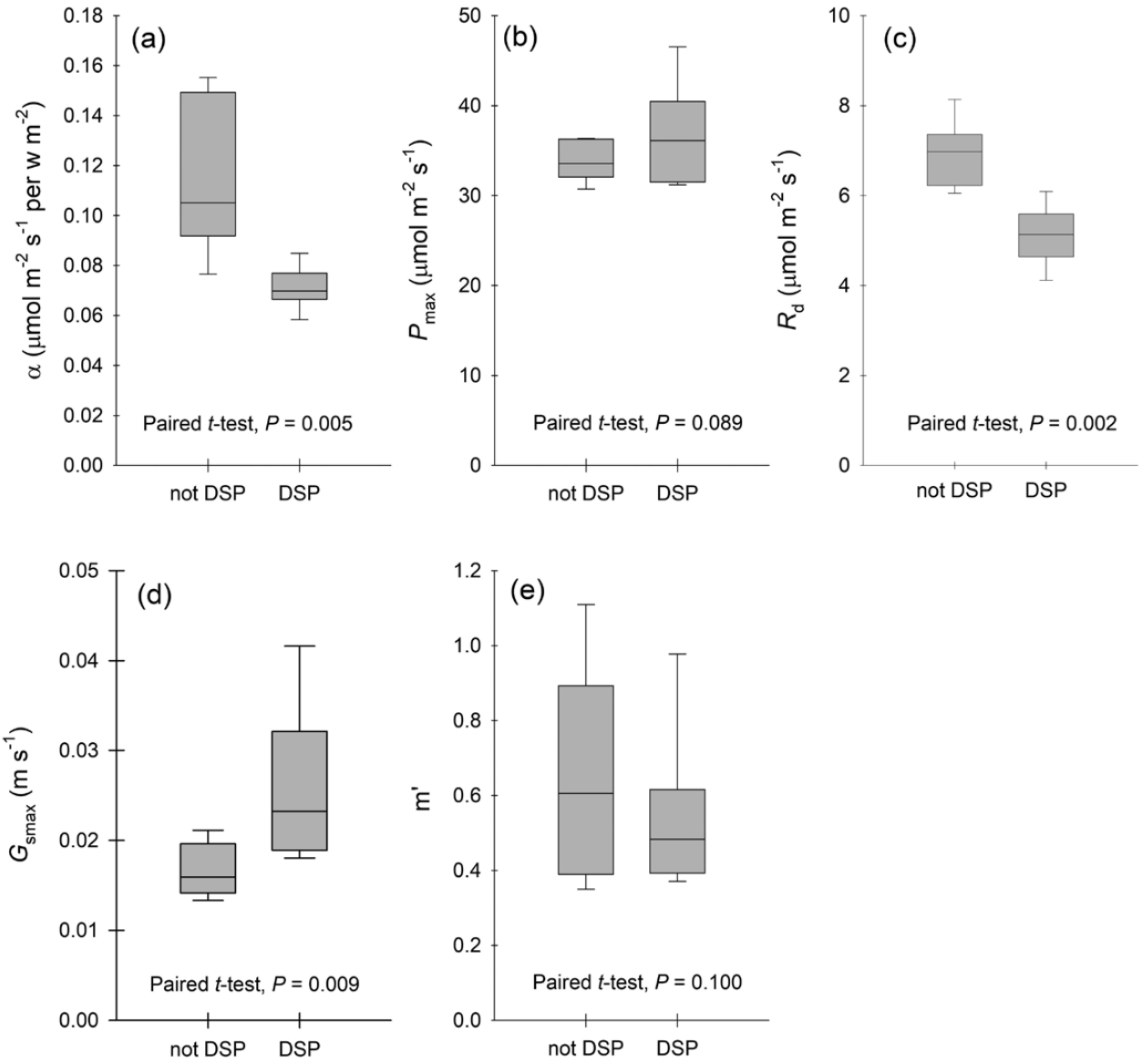

Figure 8: Comparison of ecosystem physiological properties during dry spells (DSPs) and non-DSPs at the PSO site. The definitions of dry spells and non-dry spells are provided in the text and supplementary material. (**a**) α: quantum yield; (**b**) P_{max}: light-saturated photosynthesis rate; (**c**) R_d: dark respiration; (**d**) G_{smax}: maximum surface conductance; (**e**) Q_0: a fitted parameter and m': sensitivity index.

stage contributed to a 100% GPP increase (scenario 1), while the 'rainy'-stage m' driven by 'dry'-stage light led to only a 10% increase in GPP (scenario 2). The 'dry'-stage climate (here Q, D and C_a) could contribute to a 78% GPP increase and thus played a significant role.

DISCUSSION

Tropical forests harbor a large number of species. These species are diverse in their phenologies, metabolisms and environmental responses. This diversity is amplified by tall and complex canopies. The adult trees that reach the canopy differ largely from the seedlings under the dark understory, even when they are the same species. In view of this context, when we discuss the behavior of a whole ecosystem, we are actually analyzing the bulk average characteristics of all species in different ontogenies. Here, we evaluate the adaptive strategies based on the GPP seasonality. Finally, we tried to answer the question of whether the photosynthesis of Asian tropical forests under dry conditions is limited by water stress or enhanced by increased solar radiation.

Table 2: Parameters obtained by performing curve fitting on the surface conductance responses to environmental factors.

Season	Year	G_{smax} (mm s^{-1})	Q_0	m'	r^2	n
MKL						
Cool dry	2003	7.784	449	0.152	0.060	709
	2004	8.899	916	0.196	0.074	647
Hot dry	2003	8.030	532	0.295	0.140	359
	2004	3.909	338	0.327	0.128	329
Rain season	2003	10.552	417	0.319	0.155	1059
	2004	10.100	490	0.256	0.131	1031
SKR						
Cool dry	2001	8.349	247	0.463	0.155	361
	2002	12.901	515	0.637	0.331	932
	2003	14.871	551	0.584	0.236	696
Hot dry	2001	N.A.	N.A.	N.A.	N.A.	N.A.
	2002	8.443	419	0.663	0.385	194
	2003	13.181	417	0.387	0.216	337
Rain season	2001	N.A.	N.A.	N.A.	N.A.	N.A.
	2002	22.591	882	0.331	0.289	1075
	2003	20.786	897	0.295	0.173	650
BNS						
Cool dry	2003	12.781	34	0.261	0.101	1325
	2004	11.533	26	0.320	0.153	1164
	2005	10.004	32	0.422	0.194	1328
Hot dry	2003	10.356	110	0.281	0.070	594
	2004	6.359	55	0.621	0.237	558
	2005	7.117	107	0.345	0.115	509
Rain season	2003	13.558	87	0.395	0.114	2048
	2004	17.826	201	0.651	0.220	2096
	2005	10.793	44	0.371	0.103	1958

The equation is shown in the text. G_{smax}: maximum surface conductance; Q_0: fitted parameter; m': sensitivity index; r^2: determinant of coefficient and n: number of datasets involved in curve fitting. N.A. indicates that data are not available.

Does GPP increase with light in the dry season in Asian tropical forests?

The GPP seasonality characteristics in the four studied forests can be used to classify the forests into two types, namely seasonal forests and perhumid forests. Photosynthesis was higher in the rainy season than in the dry season in all three seasonal forests: BNS, MKL and SKR (Fig. 5). The perhumid PSO forest did not exhibit clear climatic seasonality but did show a bimodal GPP pattern that corresponded to solar radiation (Figs 5 and 3).

Deriving GPP for *NEE* is a challenge for tropical forests with the smallest annual temperature ranges. Flux partitioning is highly dependent on temperature–respiration relationships (Lasslop *et al.*

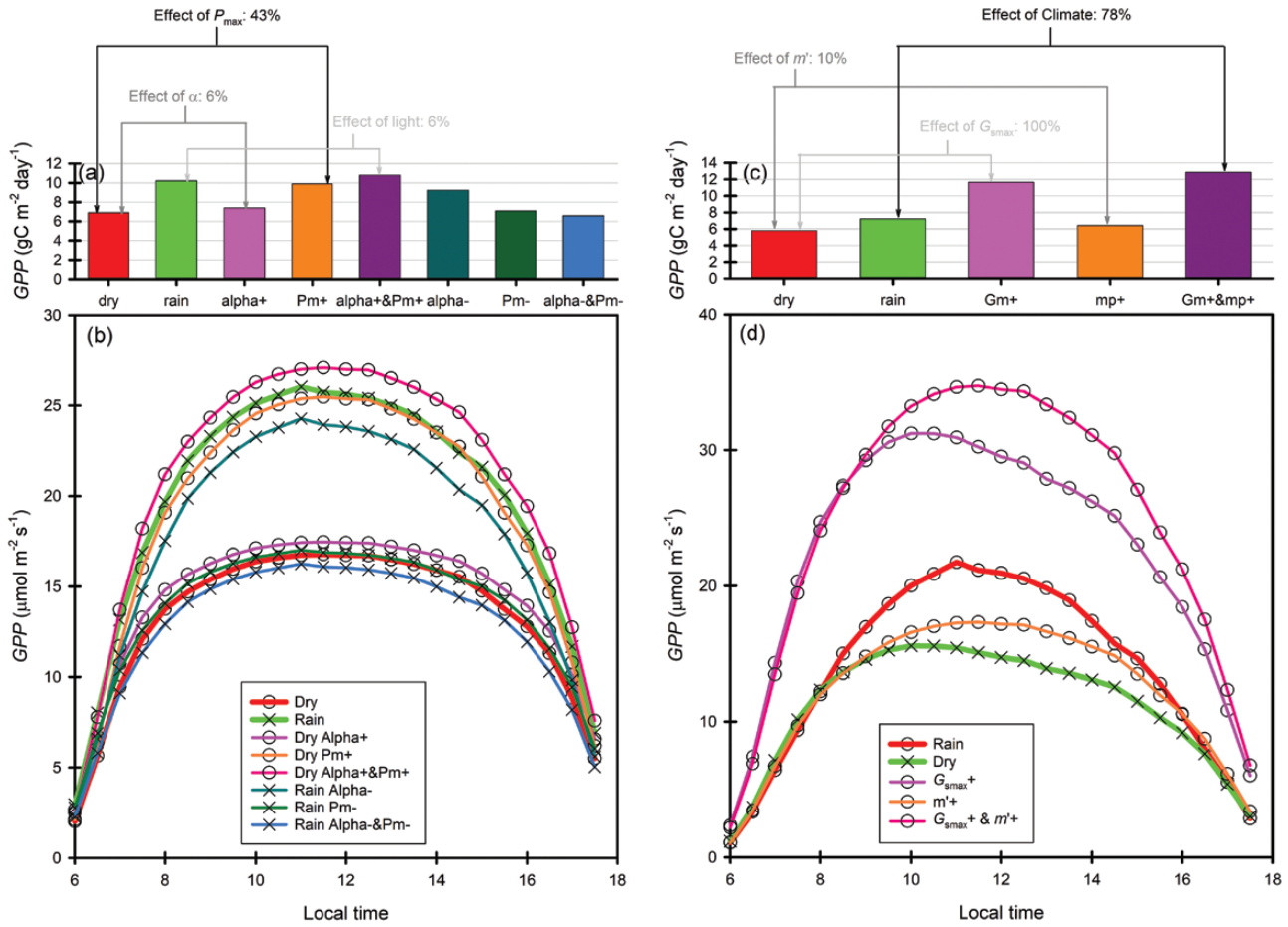

Figure 9: Light-based (**a**, **b**) and Gs-based (**c**, **d**) simulations of gross primary production (GPP) at the SKR site. Gs is the surface conductance.

2010; Reichstein *et al.* 2005), which are usually not available for evergreen tropical forests. Fortunately, we found a solution for our studied evergreen forests. First, we found a close relationship between R_d and D at the SKR site (Supplementary Fig. S2). This led to successful flux partitioning at this site. In contrast, we provide a novel method for flux partitioning at the PSO site. As reported in previous studies (Kosugi *et al.* 2008, 2012), the estimated ecosystem respiration (R_e) is approximately 5 μmol m^{-2} s^{-1} (equal to 1892 g C m^{-2} year^{-1}), as obtained by either the nighttime or daytime method. This leads to an unacceptable carbon sink for a primary tropical rainforest of 10 t C ha^{-1} year^{-1}. We found that the weak light data contaminate the daytime method-derived R_d values because R_d is highly sensitive to weak light data (Supplementary Fig. S4). After minimizing this contaminant effect, we could obtain a mean R_d value close to that reported by Kosugi *et al.* (2012), who used a delicate method. The GPP values obtained with these solid methods are also corroborated by other independent measurements. For example, the GPP values are highly correlated with the EVI results at the SKR site (Huete *et al.* 2008; Supplementary Fig. S19). The GPP at the PSO site corresponds well to the R_g values (Supplementary Fig. S21).

The driving force for GPP seasonality varied among the study sites. The seasonality of GPP was weaker than that of λE at the BNS site (Fig. 5). The relatively low R_g and T_a values in the cool-dry period significantly reduced λE but had a limited effect on GPP. This was partly because of the high LAI and photosynthetic properties (α and P_{max}) during this period (Fig. 4; Table 1). Partial leaf shedding contributed to a short (almost two-month) increase in GPP. This could be explained by the combined effect of the reviving of suppressed trees and the high photosynthesis performance of new leaves. The GPP seasonality observed at the SKR and MKL sites could be effectively explained by the EVI or LAI (Supplementary Fig. S20). The difference was that the intensive leaf shedding (Fig. 4) in the cool-dry period and the replacement with a cohort of new

leaves with strong photosynthetic performance largely enhanced photosynthesis in the rainy season at the MKL site. This finding is consistent with a previous cost–benefit analysis of deciduous and evergreen forests (Givnish 2002; Kikuzawa 1991). The bimodal GPP pattern at the PSO site is consistent with the same bimodal pattern observed for λE. Both of these patterns may have been caused by the bimodal pattern of R_g (Fig. 3).

A general comparison of GPP seasonality was performed in continental Asia and in the Brazilian Amazon. As noted by Restrepo-Coupe *et al.* (2013), equatorial tropical rainforests (5° N–5° S) exhibit increasing GPPs with the progression of the dry season. The only equatorial tropical rainforest considered in our study (PSO) received less annual rainfall (~1800 mm) than the Brazilian Amazon (>2000 mm). Nevertheless, no discernable seasonality was detected at this site, owing to the relatively evenly distributed monthly rainfall. The bimodal GPP pattern corresponded to the R_g pattern (Fig. 3), suggesting that the PSO forest is probably a water-stress-free and light-controlled ecosystem. The vegetation types corresponding to mean annual rainfall totals of 1666 mm (RJA, cited from de Sousa *et al.* 2017) and 1478 mm (PDG, cited from da Rocha *et al.* 2002) are transitional forests and savannas, respectively, in the Brazilian Amazon. Similar annual rainfall totals can support tropical seasonal forests—either deciduous or evergreen forests—in continental Southeast Asia (see the site descriptions). Although these forests all exhibited relatively high GPPs during the rainy season (in either Amazon or Asia), the forests exhibited differing degrees and durations of seasonality.

Existence of consistent adaptive strategies for Asian tropical forests to fit climate seasonality from the perspective of photosynthesis

Numerous strategies have evolved to allow forests to adapt to their biotic and abiotic environments. Here, we discussed these adaptive strategies from the perspective of photosynthesis. We hypothesized that during the rainy season, when the ecosystem is water-stress-free but light-controlled (Graham *et al.* 2003), increases in α and m' benefit ecosystem photosynthesis. In contrast, increasing the P_{max} and reducing the m' value would help forests utilize extra light in the dry season or during dry spells. These hypotheses were rejected for seasonal forests (Tables 1 and 2) but partly supported in the perhumid PSO forest (Fig. 8). The α values were significantly lower and P_{max} was higher—but not statistically significantly—during DSPs. The light inhibition of ecosystem respiration (Keenan *et al.* 2019) was also supported at the PSO site. Compared to the non-DSPs, the increased light due to reduced cloud cover during DSPs significantly reduced the R_d values (Fig. 8).

A well-recognized idea is that the new leaf benefit could play a leading role in contributing to the dry-season increase in GPP observed in Amazonian humid evergreen forests (5° S–5° N, Albert *et al.* 2018; Lopes *et al.* 2016; Wu *et al.* 2016). Although the decline in photosynthetic performance with leaf age was reported decades ago in tropical forest trees (i.e. Kitajima *et al.* 1997), it is still a new concept that this phenomenon could play a leading role in the photosynthesis of whole ecosystems with year-round evergreen leaf canopies. As reflected in the seasonal variations in Λ_{unit} (an index specifically designed for this purpose), no clear increase in the leaf photosynthetic performance was detected with the progression of the dry season in either of the two evergreen forests (Fig. 6). The lack of this pattern in the PSO forest could be explained by its perhumid climate conditions. The SKR forest, however, seems to be an exception. The seasonality is strong in this forest, and it is dominated by a monsoonal climate. The mean annual rainfall in the SKR (~1400 mm) is much lower than that in Amazonian humid forests (>2000 mm). These results suggest an unavoidable water-controlled dry season. As reported by local observers, a few trees shed their leaves in the dry season, even though these sites are called evergreen forests (Bunyavejchewin 1986). In principle, this should cause a relatively sharp increase in GPP as new leaves develop with increased photosynthetic performance; however, this was not observed at the SKR site, where GPP increases were mainly contributed by the LAI (cf. Supplementary Figs S10 and S20; a close relationship between the GPP and EVI was found). Furthermore, the new leaf benefits in deciduous forests also differed among sites. The new leaf benefit was strong and long-lasting at the MKL stie but not at the BNS site (Fig. 6). It is well known that leaf photosynthetic performance is highly correlated with leaf nitrogen (Evans 1989; Field 1983). Thus, we believe that the soil nutrient status could play a major role in the new leaf benefit phenomena. For nutrient-poor sites, maintaining evergreen or shedding a small amount of leaves is always the most economical in terms of carbon usage (Aerts 1995; Givnish 2002). The new leaf benefit is subsequently much weaker in nutrient-poor forests.

The deep water use needs to be considered when searching for a consistent adaptive strategy. However, this factor was rarely included in past studies. The soil and root depths differ largely between flood plains and mountainous forests. Root depths can reach 8 m or more in Amazonian forests (Nepstad *et al.* 1994); however, such depths are not realistic for most forests in continental Southeast Asia. The soil depths are seldom deeper than 2 m for some of the forests in Thailand and the nearby mountainous regions (Murata *et al.* 2009). Such shallow root depths reduce the potential for forests to reach deep soil water and also hamper the possible adaptive strategies that exist in deep root systems (Davidson *et al.* 2011).

We did not obtain a consistent adaptive strategy for Asian tropical forests that fit their climate seasonality. This lack of consistency was likely the result of factors other than climate conditions, such as soil nutrients, root depths and leaf phenology.

Dry season or DSP photosynthesis: water stress or light benefit?

Before the discussion, we would like to note that the use of 'water stress' or 'light controlled' here applies only to natural forests on a seasonal scale. Discerning the contribution of irregular El Niño-Southern Oscillation-related drought to photosynthesis is not our intent. If the photosynthesis of an ecosystem declines in dry conditions despite increased irradiance, we denote this as a water-limited tropical forest. Light-controlled forests are those in which ecosystem photosynthesis increases along with increased irradiance in dry conditions, regardless of the occurrence of water stress.

Clearly, the PSO forest can be viewed as a light-controlled forest. The canopy had a relatively high photosynthetic performance (Fig. 8), and the GPP exhibited a bimodal pattern consistent with that of R_g (Fig. 3). It is worth noting that G_s decreased during dry spells at this site (Fig. 7). However, this did not prevent a higher GPP from occurring in the relatively high-irradiance periods, which might have been contributed by relatively high P_{max} values. This finding acts as an exception to the suggestions of Guan *et al.* (2015) and Wagner *et al.* (2016). They suggested a threshold value of 2000 mm year^{-1}. Tropical forests growing under this threshold are probably water stressed and thus would not exhibit an increase in GPP under dry conditions. The long-term climate record demonstrated that the annual rainfall at the PSO site was well below 2000 mm year^{-1}. Favored by the even distribution of rainfall across months, the PSO site seldom experiences monthly rainfall below 100 mm. We thus cannot discern a clear dry season for the PSO site. In fact, only a small part of continental Southeast Asia receives rainfall in excess of 2000 mm year^{-1} (cf. Guan *et al.* (2015)). Therefore, a more sophisticated regime is preferred to categorize tropical forests into water-stressed or not rather than considering a single annual rainfall amount. In this new regime, the rainfall seasonality and soil nutrient status should be ranked subsequently. This was also supported by the comparison between the SKR and MKL sites. Based on the annual rainfall, the MKL site should have been more humid. Nevertheless, the MKL site experienced relatively strong rainfall seasonality. Moreover, the soil nutrients are richer at the MKL site than the SKR site. The overall result is that the MKL site is adaptively deciduous, whereas the SKR site is evergreen. The high annual rainfall sets the potential but is not sufficient to support a humid site. As reported by Suksawang *et al.* (2001), only 872.99 mm (Fig. 5, where the λE of the SKR site is clearly higher than that of the MKL site) of water evapotranspired from the ecosystem, accounting for only 53.38% of the rainfall (1635.4 mm). In other words, almost 40% of rainfall leaves this ecosystem without contributing to photosynthesis-related processes; this amount could be regarded as noneffective rainfall. The case observed at the PSO site is more efficient: the (on average) 1287 mm of rainfall evapotranspired from the ecosystem accounts for 71.34% of the annual rainfall (1804 mm, Kosugi *et al.* 2012).

According to this definition, the other three tropical forests (BNS, MKL and SKR) are water-stressed. It is not disputed that the BNS and MKL sites are water stressed, as they are either semideciduous or deciduous. The evidence for defining the SKR forest as water stressed comes from two aspects. First, SKR photosynthesis was lower in the dry season despite the enhanced irradiance (Figs 5 and 3). Second, the simulations in SKR showed that GPP was more sensitive to G_s-related processes than to light (Fig. 9). The G_s values were lower in the dry season than in the rainy season (Fig. 7). In principle, water stress acts upon photosynthesis through stomatal conductance. Thus, the SKR forest is probably water-stressed.

Supplementary Material

Supplementary material is available at *Journal of Plant Ecology* online.

Code S1: The matlab code in calculating solar radiation, this was adopted from Campbell and Norman (1998).
Code S2: The matlab code for surface conductance calculation.
Code S3: The code to obtain Rd with light-response, an example for PSO.
Code S4: The code for Gs environment response, an example for PSO dry spells.
Code S5: The matlab code for light based simulating on GPP.
Code S6: The matlab code for Gs based simulating on GPP.
Figure S1: The precipitation data for SKR site collected from published literatures.
Figure S2: The relationship between dark respiration and vapor pressure deficit used for flux partitioning in the SKR site.
Figure S3: Light response curve for SKR site.
Figure S4: A figure illustrate the weak light underestimation for PSO site.
Figure S5: The light response for PSO site.
Figure S6: The light response curve for BNS in different seasons.
Figure S7: The length of daytime for the studied 4 sites.
Figure S8: Monthly litterfall data for MKL site collected published literatures.
Figure S9: The leaf area index obtained from satellite image.
Figure S10: The time series of Gs.
Figure S11: The light response for MKL site.
Figure S12: The Gs environmental response for BNS.
Figure S13: The Gs environmental response for MKL site.
Figure S14: The Gs environmental response for SKR.
Figure S15: The Gs environmental response for PSO site.
Figure S16: An illustration that m′ could be viewed as an sensitivity index for D >1 kPa.
Figure S17: Define on the dry spells for PSO site.
Figure S18: The daytime environmental factors using to drive models simulating GPP.
Figure S19: The compassion of GPP in this study to that reported by Huete et al. 2008.
Figure S20: The compassion of GPP in this study to that reported by Huete et al. 2008.
Figure S21: The comparison of GPP estimated in this study and that of Kosugi et al. (2012).
Table S1: The *P* value for t-test in the SKR site for the light response parameters.
Table S2: The *P* value for t-test in the BNS site for the light response parameters.
Table S3: The *P* value for t-test in the SKR site for the Gs environmental response parameters.
Table S4: The *P* value for t-test in the BNS site for the Gs environmental response parameters.
Table S5: The *P* value for t-test in the MKL site for the Gs environmental response parameters.

Funding
This study was supported by the National Natural Science Foundation of China (grant nos. 41771099, 41861023 and 41861144016).

Acknowledgements
The authors wish to express their sincere thanks to the reviewers and editor for their insightful comments, suggestions and patience. The authors also acknowledge AsiaFLUX for sharing their data and the numerous people who engaged in fieldwork, instrument maintenance and data collection.

Conflict of interest statement
The authors declare that they have no conflict of interest.

REFERENCES

Aerts R (1995) The advantages of being evergreen. *Trends Ecol Evol* **10**:402–407.

Aide TM (1992) Dry season leaf production: an escape from herbivory. *Biotropica* **24**:532–537.

Albert LP, Wu J, Prohaska N, *et al*. (2018) Age-dependent leaf physiology and consequences for crown-scale carbon uptake during the dry season in an Amazon evergreen forest. *New Phytol* **219**:870–884.

Brum M, Vadeboncoeur MA, Ivanov V, *et al*. (2018) Hydrological nich segregation defines forest structure and drought tolerance strategies in a seasonal Aamzon forest. *J Ecol* **107**:318–333.

Bucci SJ, Goldstein G, Scholz FG, *et al*. (2016) Physiological significance of hydraulic segmentation, nocturnal transpiration and capacitance in tropical trees: paradigms revisited. In Glodstein G, Santiago L (eds). *Tropical Tree Physiology*. New York, USA: Springer.

Bunyavejchewin S (1983) Analysis of the tropical dry deciduous forest of Thailand, I. Characteristics of the Dominance-Types. *Nat Hist Bull Siam Soc* **31**:109–122.

Bunyavejchewin S (1986) Ecological studies of tropical semi-evergreen rain forest at Sakaerat, NakhonRatchasima, Northeast Thailand, I. Vegetation patterns. *Nat Hist Bull Siam Soc* **34**:35–57.

Campbell GS, Norman JM (1998) *An Introduction to Environmental Biophysics*. New York: Springer.

Cao M, Zou X, Warren M, *et al*. (2006) Tropical forests of Xishuangbanna, China. *Biotropica* **38**:306–309.

Chadwick R, Good P, Martin G, *et al*. (2016) Large rainfall changes consistently projected over substantial areas of tropical land. *Nat Clim Change* **6**:177–181.

Chen M, Wang G, Zhou S, *et al*. (2019) Studies on forest ecosystem physiology: marginal water-use efficiency of a tropical, seasonal, evergreen forest in Thailand. *J For Res* **30**:2163–2173.

da Rocha HR, Freitas HC, Rosolem R, *et al*. (2002) Measurements of CO_2 exchange over a woodland savanna (Cerrado Sensu stricto) in southeast Brasil. *Biota Neotropica* **2**:BN01702012002.

Dang QL, Marfo J, Du FG, *et al.* (2021) CO2 stimulation and response mechanisms vary with light supply in boreal conifers. *J Plant Ecol* **14**:291–300.

Davidson E, Lefebvre P, Brando P, *et al*. (2011) Carbon inputs and water uptake in deep soils of an eastern Amazon forest. *Forest Sci* **57**:51–58.

de Sousa CHR, Hilker T, Waring R, *et al*. (2017) Progress in remote sensing of photosynthetic activity over the Amazon basin. *Remote Sens* **9**:48.

Eamus D, Prior LD (2001) Ecophysiology of trees of seasonally dry tropics: comparisons among phenologies. *Adv Ecol Res* **32**:113–197.

Evans JR (1989) Photosynthetis and nitrogen relationships in leaves of C_3 plants. *Oecologia* **78**:9–19.

Fan S-M, Wofsy SC, Bakwin PS, *et al*. (1990) Atmosphere-biosphere exchange of CO_2 and O_3 in the central Amazon Forest. *J Geophys Res Atm* **95**:16851–16864.

Fang Q, Sha L (2006) Soil respiration in a tropical seasonal rain forest and rubber plantation in Xishuangbanna, Yunnan, SW China. *Acta Phytoecologica Sinica* **30**:97–103.

Field C (1983) Allocating leaf nitrogen for the maximization of carbon gain: leaf age as a control on the allocation program. *Oecologia* **56**:341–347.

Gamo M, Penuthai S (2005) Carbon flux observation in the tropical seasonal evergreen forest in Sakaerat, Thailand. *AsiaFlux Newsl* **14**:4–6.

Givnish T (2002) *Adaptive Significance of Evergreen vs. Deciduous Leaves: Solving the Triple Paradox*, **vol. 36**.

Goulden ML, Miller SD, da Rocha HR, *et al*. (2004) Diel and seasonal patterns of tropical forest CO_2 exchange. *Ecol Appl* **14**:42–54.

Grace J, Lloyd J, McIntyre J, *et al*. (1995) Fluxes of carbon dioxide and water vapour over an undisturbed tropical forest in south-west Amazonia. *Glob Change Biol* **1**:1–12.

Graham EA, Mulkey SS, Kitajima K, *et al*. (2003) Cloud cover limits net CO_2 uptake and growth of a rainforest tree during tropical rainy seasons. *Proc Natl Acad Sci U S A* **100**:572–576.

Guan K, Pan M, Li H, *et al*. (2015) Photosynthetic seasonality of global tropical forests constrained by hydroclimate. *Nat Geosci* **8**:284–289.

Hou H-Y (1983) Vegetation of China with reference to its geographical distribution. *Ann Mo Bot Gard* **70**:509–549.

Huete AR, Didan K, Shimabukuro YE, *et al*. (2006) Amazon rainforests green-up with sunlight in dry season. *Geophys Res Lett* **33**:L06405

Huete AR, Restrepo-Coupe N, Ratana P, *et al*. (2008) Multiple site tower flux and remote sensing comparisons of tropical forest dynamics in Monsoon Asia. *Agric For Meteorol* **148**:748–760.

Jarvis PG, Leverenz JW (1983) *Productivity of Temperate, Deciduous and Evergreen Forests*. Berlin, Heidelberg: Springer.

Jipp PH, Nepstad D, Cassel DK, *et al*. (1998) Deep soil moisture storage and transpiration in forests and pastures of seasonally-dry Amazonia. *Clim Change* **39**:395–412.

Keenan TF, Migliavacca M, Papale D, *et al*. (2019) Widespread inhibition of daytime ecosystem respiration. *Nat Ecol Evol* **3**:407–415.

Kikuzawa K (1991) A cost-benefit analysis of leaf habit and leaf longevity of trees and their geographical pattern. *Am Naturalist* **138**:1250–1263.

Kitajima K, Mulkey SS, Wright SJ (1997) Decline of photosynthetic capacity with leaf age in relation to leaf longevities for five tropical canopy tree species. *Am J Bot* **84**:702–708.

Kosugi Y, Takanashi S, Ohkubo S, *et al*. (2008) CO_2 exchange of a tropical rainforest at Pasoh in Peninsular Malaysia. *Agric For Meteorol* **148**:439–452.

Kosugi Y, Takanashi S, Tani M, *et al*. (2012) Effect of inter-annual climate variability on evapotranspiration and canopy CO_2 exchange of a tropical rainforest in Peninsular Malaysia. *J Forest Res* **17**:227–240.

Lasslop G, Reichstein M, Papale D, *et al*. (2010) Separation of net ecosystem exchange into assimilation and respiration using a light response curve approach: critical issues and global evaluation. *Glob Change Biol* **16**:187–208.

Leigh Jr EG (1999) *Tropical Forest Ecology: A View from Barro Colorado Island*. New York: Oxford University Press.

Lopes AP, Nelson BW, Wu J, *et al*. (2016) Leaf flush drives dry season green-up of the central Amazon. *Remote Sens Environ* **182**:90–98.

Markewitz D, Devine S, Davidson E, *et al*. (2010) Soil moisture depletion under simulated drought in the Amazon: impacts on deep root uptake. *New Phytol* **187**:592–607.

Marod D, Kutintara U, Yarwudhi C, *et al*. (1999) Structural dynamics of a natural mixed deciduous forest in Western Thailand. *J Veg Sci* **10**:777–786.

Medlyn BE, Duursma RA, Eamus D, *et al*. (2011) Reconciling the optimal and empirical approaches to modeling stomatal conductance. *Glob Change Biol* **17**:2134–2144.

Monsi M, Saeki T (2005) On the factor light in plant communities and its importance for matter production. *Ann Bot* **95**:549–567.

Murata N, Ohta S, Ishida A, *et al*. (2009) Comparison of soil depths between evergreen and deciduous forests as a determinant of their distribution, Northeast Thailand. *J Forest Res* **14**:212–220.

Myneni RB, Yang W, Nemani RR, *et al*. (2007) Large seasonal swings in leaf area of Amazon rainforests. *Proc Natl Acad Sci U S A* **104**:4820–4823.

Nepstad DC, de Carvalho CR, Davidson EA, *et al*. (1994) The role of deep roots in the hydrological and carbon cycles of Amazonian forests and pastures. *Nature* **372**:666–669.

Oren R, Sperry JS, Katul GG, *et al*. (1999) Survey and synthesis of intra- and interspecific variation in stomatal sensitivity to vapour pressure deficit. *Plant Cell Environ* **22**:1515–1526.

Phillips OL, Aragão LEOC, Lewis SL, *et al*. (2009) Drought sensitivity of the Amazon rainforest. *Science* **323**:1344–1347.

Pinker RT, Thompson OE, Eck TF (1980) The energy balance of a tropical evergreen forest. *J Appl Meteorol* **19**:1341–1350.

Reichstein M, Falge E, Baldocchi D, *et al*. (2005) On the separation of net ecosystem exchange into assimilation and ecosystem respiration: review and improved algorithm. *Glob Change Biol* **11**:1424–1439.

Restrepo-Coupe N, da Rocha HR, Hutyra LR, *et al*. (2013) What drives the seasonality of photosynthesis across the Amazon basin? A cross-site analysis of eddy flux tower measurements from the Brasil flux network. *Agric For Meteorol* **18**:128–144.

Rundel PW, Boonpragob K (1995) *Dry Forest Ecosystems of Thailand*. New York: Cambridge University Press.

Rundel PW, Boonpragob K, Patterson M (2017) Seasonal water relations and leaf temperature in a deciduous dipterocarp forest in Northeastern Thailand. *Forests* **8**:368.

Saleska SR, Miller SD, Matross DM, *et al*. (2003) Carbon in Amazon forests: unexpected seasonal fluxes and disturbance-induced losses. *Science* **302**:1554–1557.

Saleska SR, Wu J, Guan KY, *et al*. (2016) Dry-season greening of Amazon forests. *Nature* **531**:E4–E5.

Sha L, Zheng Z, Tang J-W, *et al*. (2005) Soil respiration in tropical seasonal rain forest in Xishuangbanna, SW China. *Sci China Ser D Earth Sci* **48**:189–197.

Suksawang S, Tangtham N, Panuthai S (2001) *Water Balance of Natural Forest and Mixed Forest Plantation Watershed at Mae Klong Head Watershed Area, Kanchanaburi Province*. http://agris.fao.org/agris-search/search.do?recordID=TH2003000724, 44–54.

Suriyapong Y (2003) Study of ground dewelling ant populations and their relationship to some ecological factors in Sakaerat environmental research station, NakhonRatchasima. *PhD Thesis*. Suranaree University of Technology.

Swinbank WC (1951) The measurement of vertical transfer of heat and water vapor by eddies in the lower atmosphere. *J Meteorol* **8**:135–145.

Takahashi M, Hirai K, Limtong P, *et al*. (2011) Topographic variation in heterotrophic and autotrophic soil respiration in a tropical seasonal forest in Thailand. *Soil Sci Plant Nutr* **57**:452–465.

Tan Z-H, Zhao J-F, Wang G-Z, *et al*. (2019) Surface conductance for evapotranspiration of tropical forests: calculations, variations, and controls. *Agric For Meteorol* **275**:317–328.

Tang H, Dubayah R (2017) Light-driven growth in Amazon evergreen forests explained by seasonal variations of vertical canopy structure. *Proc Natl Acad Sci U S A* **114**:2640–2644.

Terakunpisut J (2003) Carbon sequestration potential in aboveground biomass of Thong PhaPhum forest ecosystem. *Master Thesis*. Chulalongkorn University.

Ueda MU, Kachina P, Marod D, *et al*. (2017) Soil properties and gross nitrogen dynamics in old growth and secondary forest in four types of tropical forest in Thailand. *Forest Ecol Manag* **398**:130–139.

Wagner FH, Hérault B, Bonal D, *et al*. (2016) Climate seasonality limits leaf carbon assimilation and wood productivity in tropical forests. *Biogeosciences* **13**:2537–2562.

Wehr R, Munger JW, McManus JB, *et al*. (2016) Seasonality of temperate forest photosynthesis and daytime respiration. *Nature* **534**:680–683.

Wright SJ, Cornejo FH (1990) Seasonal drought and leaf fall in a tropical forest. *Ecology* **71**:1165–1175.

Wright SJ, van Schaik CP (1994) Light and the phenology of tropical trees. *Am Naturalist* **143**:192–199.

Wu J, Albert LP, Lopes AP, *et al*. (2016) Leaf development and demography explain photosynthetic seasonality in Amazon evergreen forests. *Science* **351**:972–976.

Wu J, Serbin SP, Ely KS, *et al*. (2020) The response of stomatal conductance to seasonal drought in tropical forests. *Glob Change Biol* **26**:823–839.

Xiao X, Zhang Q, Saleska S, *et al*. (2005) Satellite-based modeling of gross primary production in a seasonally moist tropical evergreen forest. *Remote Sens Environ* **94**:105–122.

Yada Y, Kira T (1982) Accumulation of organic matter, carbon, nitrogen and other nutrient elements in the soils of lowland rainforest at Pasoh, Peninsular Malaysia. *Jpn J Ecol* **32**:275–291.

Yamashita T, Kasuya N, Wan Rasidah, K, *et al*. (2003) *Soil and Belowground Characteristics of Pasoh Forest Reserve*. Tokyo, Japan: Springer.

Yan H, Wang S-Q, da Rocha HR, *et al*. (2017) Simulation of the unexpected photosynthetic seasonality in Amazonian evergreen forests by using an improved diffuse fraction-based light use efficiency model. *J Geophys Res Biogeosci* **122**:3014–3030.

Yoda K (1983) Three-dimensional distribution of light intensity in a tropical rain forest of West Malaysia. *Jpn J Ecol* **24**:247–254.

Yoda K, Nishioka M (1982) Soil respiration in dry and wet seasons in a tropical dry-evergreen forest in Sakaerat, NE Thailand. *Jpn J Ecol* **32**:539–541.

Yoda K, Nishioka M, Dhanmanonda P (1983) Vertical and horizontal distribution of relative illuminance in the dry and wet season in a tropical dry-evergreen forest in Sakareat, NE Thailand. *Jpn J Ecol* **33**:97–100.

Zhang K (1963) A preliminary analysis on climatic properties of South Yunnan and its possible controlling factors. *Acta Meteorological Sinica* **33**:218–230.

Zhang J, Cao M (1995) Tropical forest vegetation of Xishuangbanna, SW China and its secondary changes, with special reference to some problems in local nature conservation. *Biol Conserv* **73**:229–238.